ORIGINAL ARTICLE

Kinetically controlled formation of uniform FePO$_4$ shells and their potential for use in high-performance sodium ion batteries

Shu-Yi Duan[1,2], Jun-Yu Piao[1,2], Tian-Qi Zhang[1,2], Yong-Gang Sun[1,2], Xiao-Chan Liu[1,2], An-Min Cao[1,2] and Li-Jun Wan[1,2]

Amorphous iron phosphates are potential cathode materials for sodium ion batteries. The amorphous FePO$_4$ matrix is able to insert/extract sodium ions reversibly without apparent structural degradation, resulting in stable performance during the charge/discharge process. However, the extremely low electronic conductivity of FePO$_4$ itself becomes a formidable obstacle for its application as a high-performance cathode material. Here, by tuning the growth kinetics of FePO$_4$ in an aqueous solution, we were able to control its formation onto a large variety of substrates, forming uniform core-shell structures. Specifically, the use of multiwalled carbon nanotubes as the core material together with the growth control of FePO$_4$ produced the core-shell structure of MWCNTs@FePO$_4$ with a delicately controlled shell thicknesses. We confirmed that such a nanocomposite can act as an effective cathode material by taking advantage of both the highly conductive core and the electrochemically active shell, leading to improved battery performance as revealed by the high discharge capacity and the greatly improved rate capability. We anticipate that our progress in FePO$_4$ control offers new potential in different research fields, such as materials chemistry, catalysis and energy storage devices.

INTRODUCTION

Sodium ion batteries (SIBs) are potential candidates for large-scale energy storage devices owing to their evident advantages, including low cost, wide availability and environmental friendliness.[1–5] Owing to the much larger size of the sodium ion compared with the lithium ion, the identification of a suitable intercalation electrode material that can ensure reversible intercalation/extraction of sodium ions without an apparent volume change or structural degradation has been long pursued.[6–8] Amorphous iron phosphates have been identified as a promising cathode material for SIBs in view of their unique properties. Compared with its crystalline counterpart, the amorphous framework of FePO$_4$ is defect free, can provide more available sites for Na ions and can exhibit less structural confinement to the reversible insertion/extraction for Na ions,[9–11] which ensure a much improved structural stability over long-term cycling. Unfortunately, iron phosphates themselves are well known for their poor electronic conductivity,[12,13] leading to sluggish electron transport during cycling, which becomes a critical issue in the consideration of FePO$_4$ as a practical cathode material.

For the application of FePO$_4$ as a possible cathode material, it is of great importance that the structure of the electrode material is well tailored to alleviate the polarization issue. Generally, two different approaches have been used to facilitate electron transport. Obviously, the introduction of a highly conductive matrix to form a composite material becomes a logical and reasonable approach to achieve higher electron conductivity.[14–18] For example, Liu *et al.*[10] showed that a mixture of single-walled carbon nanotubes and FePO$_4$ nanoparticles showed much improved battery performance and high cyclability. single-walled carbon nanotubes are a highly connected network that can facilitate the electron transport of embedded FePO$_4$ particles. Meanwhile, the structural control of the FePO$_4$ phase itself is effective for achieving improved kinetics and support FePO$_4$ as a possible electrode material.[19,20] For example, Fang *et al.*[9] demonstrated that mesoporous FePO$_4$ nanospheres with conductive carbon exhibit a higher discharge capacity and better cycle stability. It has been proposed that the mesopores of FePO$_4$ are a favorable transport path for metal ions, leading to faster intercalation kinetics of Na ions for better battery properties.

The core-shell structure has been known as a very attractive tool box in material design and functionalization.[21–23] A suitable combination of two functional materials as the core and the shell makes it possible to take advantage of the merits of the two contributing parts to provide an optimized performance.[21,24] Notably, a cable-like structure with a coaxial configuration has shown great

success in addressing the issue of conduction of the surface material.[18,25,26] The inner conductive core wire can act as an effective transport pathway to achieve enhanced electrochemical kinetics in such a unique nanocomposite, which obviously provides much better contact between the core and the shell compared with a simple mixture of these two components. It is therefore anticipated that a core-sheath structure with FePO$_4$ as the outside coating layer can be beneficial for battery applications when a conductive phase is at the core. Unfortunately, the controlled deposition of metal phosphates, or FePO$_4$ as discussed in this contribution, onto a preexisting substrate via a heterogeneous growth method in solution is an ongoing challenge. The low solubility of FePO$_4$ in solution ($K_{sp} = 1.3 \times 10^{-22}$ at 25 °C) results in rapid precipitation and self-nucleation into independent particles in addition to pre-added seeds, leading to a failure to form core-shell structures. The atomic layer deposition technique can form well-defined shells of FePO$_4$ by controlling the thin film growth in a reaction chamber.[27,28] Unfortunately, the atomic layer deposition process is also notorious in terms of its high cost, limited large-scale production, tedious operation and risky precursor chemistry. Regarding the coating strategy, the layer-by-layer assembly protocol of immersing seeds into solutions of desired materials has been a successful practice for anchoring different species.[29] However, such an immersion process is also well known for its shortcomings; the process is time consuming and it must be carefully operated to produce a satisfactory coating. Kim *et al.*[18] reported a synthetic strategy to construct the core-shell structure of MWCNTs@FePO$_4$, which required the alternate immersion of the substrate material into an Fe^{3+} solution and a H$_2$PO$_4^-$ solution several times. FePO$_4$ coating layers were able to grow onto the surface of substrates through this process, but it was time consuming and difficult to scale up. Therefore, a simple, low-cost synthetic protocol to construct a uniform FePO$_4$ coating is in high demand to fulfill its potential as a possible electrode material in SIBs.

Herein, we report our progress on the controlled formation of FePO$_4$-based core-shell structures using a simple and straightforward synthetic protocol. By tuning the growth kinetics during FePO$_4$ formation, we succeeded in depositing FePO$_4$ nanoshells onto a large variety of substrates, forming uniform core-shell structures with different cores. We show that the shell thickness of the FePO$_4$ layer can be accurately controlled by tuning the reaction parameters. Using multiwalled carbon nanotubes (MWCNTs) as the conducting core, we prepared cathode materials of MWCNTs@FePO$_4$ with a well-controlled surface shell, which were then used as a model system to investigate their potential in SIBs. We identified that the core-shell structured electrode material with a 4-nm FePO$_4$ surface shell delivered the best battery performance, as demonstrated by its high cycle stability and rate capacity.

EXPERIMENTAL PROCEDURES

Materials
Iron nitrate, nitric acid, disodium hydrogen phosphate and urea were of analytical purity and purchased from Sinopharm Chemical Reagent Co., Ltd. (Shanghai, China) SnO$_2$ nanoparticles, silicon nanospheres and MWCNTs were purchased from Beijing DK Nanotechnology Co., Ltd (Beijing, China). The MWCNTs were treated with mixed acids to facilitate their dispersion in water, whereas other nanoparticles were used as received. Milli-Q water (resistance > 18 MΩ) was used for all experiments. All chemicals were used as received without further purification.

Synthesis
Fe(NO$_3$)$_3$·9H$_2$O, HNO$_3$, Na$_2$HPO$_4$·12H$_2$O and CO(NH$_2$)$_2$ were dissolved in 30.0 ml of distilled water under mechanical magnetic stirring. The pH was

titrated to 1 to ensure a clear solution. The core material was added to the solution as a seed and then incubated at 80 °C for 20 h. The obtained product was separated from the solution by centrifuging at 10 000 r.p.m. for 5 min, washing with water and ethanol, drying at 80 °C for 10 h, and sintering at 400 °C for 5 h to remove crystal water. By tuning the ratio of the reactants and core material, core-shell structures with different shell thicknesses were obtained.

Material characterization
Transmission electron microscopy (TEM) and high-resolution transmission electron microscopy (HRTEM) images were recorded on JEOL-2100F and FEI Tecnai F20 instruments operated at 200 kV. Thermogravimetric tests were conducted on a DTG-60 instrument at temperatures ranging from room temperature to 800 °C in an air atmosphere. X-ray diffraction (XRD) data were collected on a Rigaku D/MAX-2500 instrument with Cu K_α radiation at 50 kV and 250 mA. X-ray photoelectron spectroscopy data were acquired on an ESCALAB 220i-XL electron spectrometer from VG Scientific using 300 W Al Kα radiation. The inductively coupled plasma-atomic emission spectroscopy experiments were conducted on an Shimadzu instrument (ICPE-9000).

Electrochemical measurements
Charge–discharge tests were performed with CR2032 coin cells assembled in an argon-filled glove box, which consisted of a sodium metal as the counter and reference electrodes, a cathode as the working electrode, 1 M NaClO$_4$ in ethylene carbonate (EC)/diethyl carbonate (DEC) (1:1:1, in wt.%) as the electrolyte, and a glass fiber membrane (Whatman, Maidstone, UK) as the separator. The cathode was prepared as a mixed slurry of 60 wt.% active materials, 20 wt.% Super P carbon black and 20 wt.% polyvinylidene fluoride (Sigma-Aldrich, St Louis, MO, USA) binder in an n-methyl pyrrolidone solvent. This mixture was cast onto Al foil (99%, Goodfellow, Cambridge, UK) and cut into circular electrodes with an area of 1.13 cm^2 after drying under vacuum at 80 °C for 10 h. Galvanostatic tests of the assembled cells were performed using a Land CT2001A battery test system with a voltage window of 1.5–4.2 V at room temperature. Cyclic voltammograms and electrochemical impedance spectroscopy data were obtained using an Autolab test system.

RESULTS AND DISCUSSION
Briefly, an aqueous solution of 4 mM Fe(NO$_3$)$_3$ was used as the iron source, and its pH was adjusted to approximately 1 to prevent direct precipitation of FePO$_4$ upon the addition of 4 mM Na$_2$HPO$_4$. Urea was selected as the pH controller due to its special ability to gradually release OH$^-$ when heated at approximately 80 °C. Thus, it became possible to slowly form the FePO$_4$ in a controllable way as a core-shell structure rather than via rapid precipitation into independent particles. Polystyrene (PS) nanospheres were used as seeds for the growth of FePO$_4$. The uniform size and shape of the PS spheres made them a preferable choice for the observation of the surface layer and for the systematic evaluation of the coating effect. Figure 1a shows a representative TEM image of the freshly prepared PS nanospheres, which were approximately 500 nm in size and smooth on the surface. Heating of the solution initialized urea hydrolysis, resulting in an increase in the pH of the solution and then the precipitation of FePO$_4$. As shown in Figure 1b, the existence of 100 mg of PS seeds in the solution led to the formation of a very thin FePO$_4$ surface layer, forming a typical core-shell structure of PS@FePO$_4$ with a continuous and uniform distribution on the outer layer. The HRTEM image shown in the inset of Figure 1b confirmed that the FePO$_4$ nanoshell was approximately 10 nm in thickness. The surface shell was amorphous in nature with no obvious lattice fringe observed, as revealed by the HRTEM investigation. The scanning electron microscopy characterization of the PS spheres before and after coatings (Supplementary Figures S1a and b) showed that nanospheres were the only morphology present for these two samples. It was
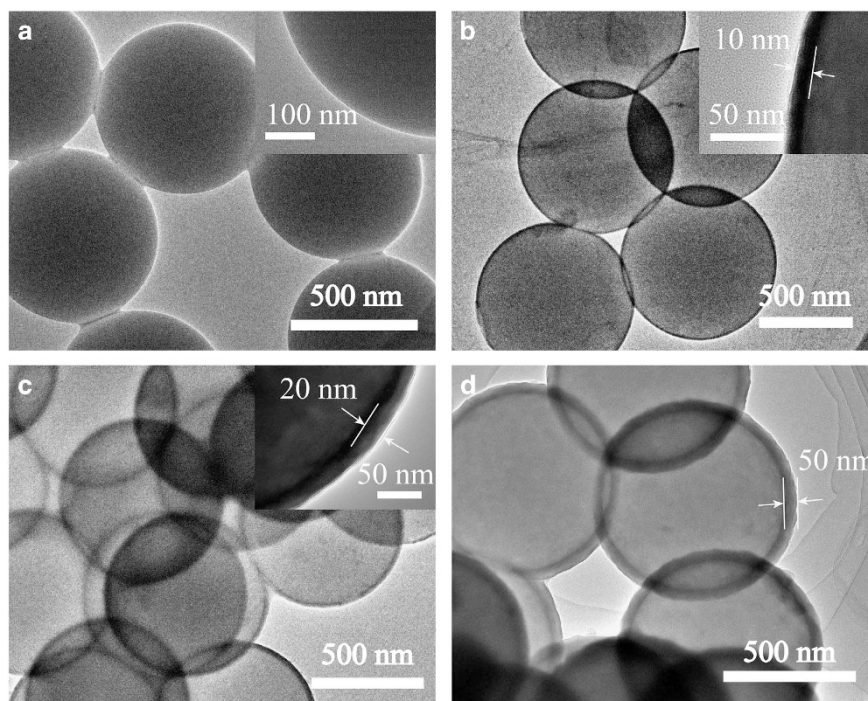
Figure 1 TEM images of the freshly produced PS (**a**) and surface-coated PS (**b–d**). The thicknesses of the coating layers were 10 nm (**b**), 20 nm (**c**), 50 nm (**d**), which were achieved by changing the amounts of PS seeds and maintaining the concentration of Fe^{3+} and PO_4^{3-} precursors. The concentrations of Fe^{3+} and PO_4^{3-} were 4 mM, and the amounts of PS were 100 mg for the 10-nm surface coating, 75 mg for the 20-nm surface coating and 45 mg for the 50-nm surface coating. PS, polystyrene; TEM, transmission electron microscopy.

expected that the $FePO_4$ would form in the solution as the surface layer and that no other phase of independent $FePO_4$ particles would exist. The XRD pattern of the collected powder showed no obvious peaks, revealing that the sample was amorphous in nature, which was in good agreement with the HRTEM result. Elemental analysis of the particles was also conducted via scanning TEM. As shown in Supplementary Figure S2, different elements, including Fe, P and O, were homogeneously distributed around the PS surface, further confirming the formation of the PS@$FePO_4$ structure.

We found that such a synthetic route could be a very convenient platform for the control of the core-shell structure. Typically, the shell thickness of $FePO_4$ can be easily tuned by simply changing the reaction parameters, such as the amount of PS seeds and the reactant concentrations. Unsurprisingly, a reduction in the amount of PS seeds as the other conditions remained unchanged in solution produced a thicker surface layer. As shown in Figure 1c, a much thicker $FePO_4$ shell of approximately 20 nm in thickness was confirmed (inset of Figure 1c) and was prepared when less PS (75 mg) was introduced as the substrate for $FePO_4$ growth. This trend became even more obvious when the PS amount was further reduced. Figure 1d shows the appearance of a much thicker $FePO_4$ surface layer that was 50 nm in thickness when there was 45 mg of PS. Furthermore, we also found that a change in the reactant concentrations, namely, those of $Fe(NO_3)_3$ and Na_2HPO_4, were very effective for the control of the core-shell structures, with no discernible phase separations between PS and $FePO_4$, as shown in Supplementary Figure S3. The obtained $FePO_4$ shells were amorphous, as shown in Supplementary Figure S4, there were no obvious peaks in the XRD pattern of PS@$FePO_4$ sample.

The removal of the PS core produced pure $FePO_4$. Figure 2a shows the emergence of hollow nanospheres when the sample was heated to 500 °C in an air flow. The elemental mapping (Figures 2b–d) of

randomly picked particles in scanning TEM mode revealed the uniform distributions of different elements, including Fe, P and O, respectively, across the wall of the particles. X-ray photoelectron spectroscopy analysis also identified the existence of these three elements, as shown in Figures 2e–g. Although the sample still remained amorphous after heating to 500 °C, it could be transferred into pure crystalline $FePO_4$ if heated to a temperature as high as 800 °C (HRTEM, electron diffraction pattern and XRD pattern of crystalline $FePO_4$ were in Supplementary Figures S5b–d, respectively[30]). Such a high-temperature treatment sintered the particles into large microsized particles with irregular shapes (Supplementary Figure S5a). All these characterizations together confirmed the formation of amorphous $FePO_4$ as a result of the reaction control, which formed a uniform core-shell structure instead of a simple mixture of two independent phases.

Our synthetic protocol provides a very flexible platform for the construction of different core-shell structures via simply changing the seeds used for further growth. No surface modification of the core materials was necessary, and the $FePO_4$ could be easily deposited onto a large variety of substrates, including semiconductors, metal oxides, metal and carbon compounds. Figure 3 shows representative TEM images of the seeds used, including SnO_2 particles (Figure 3a), silicon particles (Figure 3b), gold particles (Figure 3c) and MWCNTs (Figure 3d). Similar to the observation of PS nanospheres, an amorphous $FePO_4$ surface layer formed around these seeds despite their obvious differences in size and shape. Typically, as shown in Figure 3d, we observed the existence of a 12-nm $FePO_4$ layer wrapping around the tubular structure of the MWCNTs. The HRTEM image in the inset of Figure 3d confirmed the uniformity of the surface shell on the crystalline carbon substrate. Similarly, it was also possible to
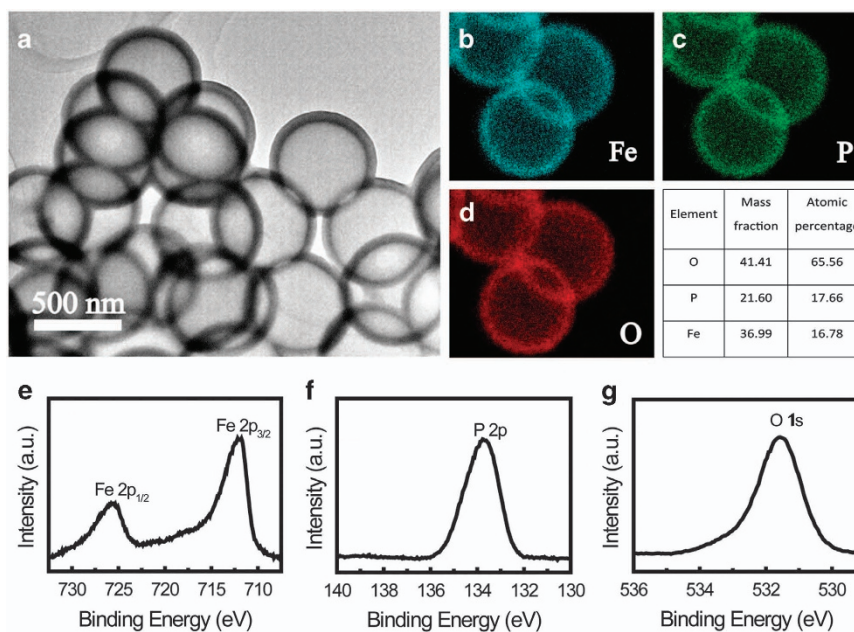
4

Element	Mass fraction	Atomic percentage
O	41.41	65.56
P	21.60	17.66
Fe	36.99	16.78

Figure 2 STEM images (**a–e**) and XPS characterization (**e–g**) of FePO₄ hollow spheres obtained by sintering at 500 °C for 5 h in air: TEM morphology (**a**); elemental mappings of Fe (**b**), P (**c**) and O (**d**); and XPS spectra (**e–g**) of Fe 2p (**e**), P 2p (**f**), and O 1s (**g**). STEM, scanning transmission electron microscopy; TEM, transmission electron microscopy; XPS, X-ray photoelectron spectroscopy.
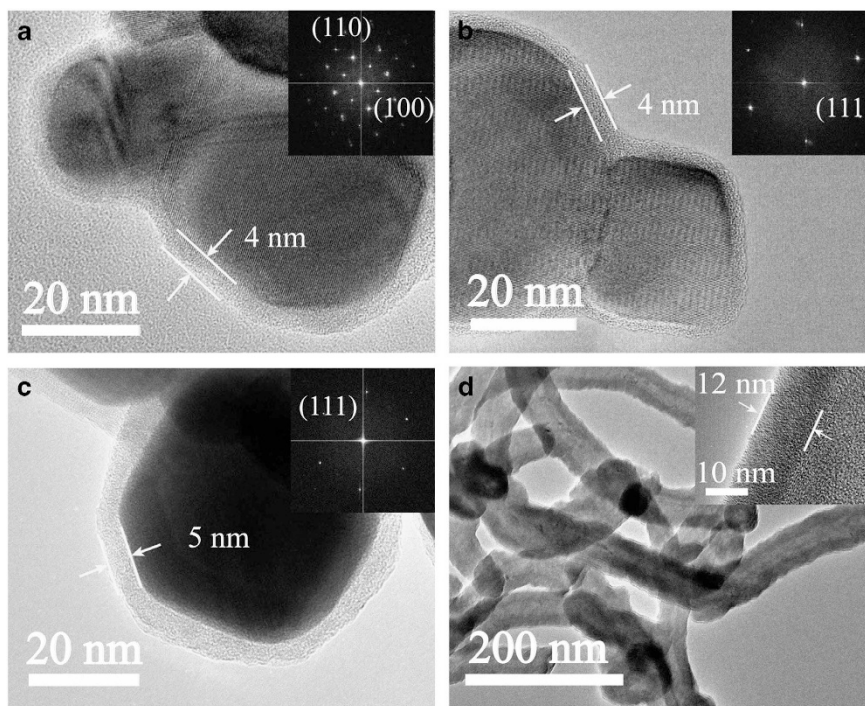

Figure 3 TEM images of the various substrate materials with different thicknesses of iron phosphates nanoshells: SnO₂@4 nm FePO₄ (**a**), Si@4 nm FePO₄ (**b**), Au@5 nm FePO₄ (**c**) and MWCNTs@12 nm FePO₄ (**d**). TEM, transmission electron microscopy.

tune the thickness of the FePO₄ layer via a concerted effort of reaction control.

For the deposition of FePO₄ on preexisting substrates in solution, it was essential to follow a heterogeneous growth route to achieve a core-shell structure. Otherwise, the homogeneous precipitation of FePO₄ itself self-nucleated and then grew into independent particles aside from the seeds, forming a mixture of two separate phases rather than a single phase of core-shell particles. To ensure a favorable precipitation of the surface coating, we found that the following two critical conditions must be satisfied: (1) acidic conditions in the starting solution to prevent the direct precipitation of Fe^{3+} and PO_4^{3-} and (2) the use of urea as a special pH controller during the reaction to mediate the growth kinetics of FePO₄ due to its unique capability to gradually release OH^- upon heating. In our synthesis, we

started the reaction under acidic conditions with the pH value controlled as low as 1. Otherwise, Fe^{3+} and PO_4^{3-} would rapidly nucleate and precipitate into separate particles due to the low solubility of iron phosphates (1.3×10^{-22} at 25 °C) as shown in Figure 6d. Supplementary Figure S6a shows a TEM image of the sample prepared with no pH control, whereby FePO$_4$ formed irregular particles in addition to the PS cores. Our experiment showed that the use of urea as an agent for growth control was of equal importance if a core-shell structure was expected. Compared with precipitants such as NaOH and NH$_3$·H$_2$O, which caused an immediate increase in the OH$^-$ concentration and accordingly a fast consumption of H$^+$ in solution (Supplementary Figures S6b and c), urea slowly hydrolyzed to gradually release OH$^-$ during the heating process. Thus, the acidic conditions of the solution could be slowly changed, leading to the formation of FePO$_4$ in a more controllable way. Such a control of the growth kinetics made heterogeneous growth possible due to the successful inhibition of the fast nucleation process, producing only core-shell-structured precipitates rather than separate particles.

Inspired by the uniform core-shell structure of FePO$_4$-based materials, we expected that they could be used as potential cathode materials for SIBs if the conductivity issue could be properly addressed by using a suitable core material. Accordingly, we selected highly conductive MWCNTs as the substrate to build a cable-like structure to ensure good electron conductivity of the composite materials. The construction of a core-shell structure of MWCNTs@FePO$_4$ made it possible to combine the advantages of both the conductive core and the active amorphous layer, which is favorable, especially for the use of cathode materials at high charge/discharge currents or at a high c-rate. For the amorphous FePO$_4$ surface layer, Na ions could diffuse through the network and insert/extract without apparent volume change or structural degradation. Meanwhile, the interconnecting MWCNTs formed fast electron transport pathways, which facilitated the electron transport within the FePO$_4$ layers. In addition, the intimate connection between FePO$_4$ and the MWCNTs in the core-shell-structured MWCNTs@FePO$_4$ contributed to much better electrochemical kinetics through the interface. Thus, MWCNTs@FePO$_4$ was anticipated to considerably enhance battery performance by improving the conductivity of both Na ions and electrons.

To systematically evaluate the performance of the core-shell structure, we carried out a series of syntheses to control the structure of FePO$_4$ on the surface. Using the benefits of the convenience of our synthetic protocol, it became simple and effective for us to delicately control the uniformity and thickness of the FePO$_4$ shells around the MWCNTs, giving us a good model system for the optimization of their battery performance. Supplementary Figure S7 shows the core-shell structures of the MWCNTs@FePO$_4$ that we prepared, with the thickness of the FePO$_4$ shell precisely controlled at 4, 6 and 12 nm. Different kinds of analyses, including thermogravimetric analysis, inductively coupled plasma-atomic emission spectroscopy, XRD and Raman spectroscopy, were conducted to characterize these samples. The thermogravimetric analysis result (shown in Supplementary Figures S8a–c) provided a rough estimation of the FePO$_4$ content in these shell-controlled samples. The weight percentages of FePO$_4$ were approximately 75.8, 82.7 and 90%, respectively. The inductively coupled plasma-atomic emission spectroscopy results also show that the FePO$_4$ contents were 75.08, 84.38 and 89.47% for the 4, 6 and 12-nm-coated samples, respectively (Supplementary Table S1). The XRD pattern of MWCNTs@FePO$_4$ (Supplementary Figure S8d) showed no obvious crystalline peaks, indicating the amorphous nature of the FePO$_4$ surface layer, which was consistent with the TEM images.

The Raman spectra (Supplementary Figure S9) of a representative sample that had a 4-nm FePO$_4$ shell on the surface exhibited typical peaks at 1340, 1567 and 2677 cm^{-1} which were fingerprint vibrations originating from the D band, G band and 2D band, respectively, of carbon.[31] The high ratio of the peak area of the D band to the G band ($I_D/I_G = 0.99$) and the existence of the 2D band both confirmed that the core material of MWCNTs had a highly ordered graphene structure.[32] Therefore, a high electron conductivity for the core-shell structured sample due to the carbon nanotube core as a conductive cable was expected.

The battery performances of the MWCNTs@FePO$_4$ samples were examined for a CR2032 coin cell using sodium as the counter electrode. First, cyclic voltammetry measurements were used to study the electrochemical reaction of the MWCNTs@FePO$_4$ samples (Supplementary Figure S10). As shown in a typical cyclic voltammetry curve of the MWCNTs@FePO$_4$, there was a pair of redox peaks located at approximately 2.8 and 2.2 V, which could be attributed to the characteristic redox reactions between Na and FePO$_4$, respectively.[9] For the amorphous FePO$_4$ cathode, the cyclic voltammetry curve showed broad peaks during the reduction and oxidation process, indicating that the electrochemical insertion/extraction of the cations proceeded in a large number of successive Na$_x$FePO$_4$ phases without the formation of highly crystalline phases. We also performed *ex situ* XRD experiments on the FePO$_4$ sample during different states of the charge/discharge process (shown in Supplementary Figure S11). In addition to the peaks due to the Al foil, we did not observe any obvious peaks due to the reduction/oxidation of the cathode materials, indicating that the FePO$_4$ sample remained mostly amorphous during its interaction with Na$^+$.[33]

We, thereafter, tested the battery performance of the shell-controlled MWCNTs@FePO$_4$ samples to gain a better understanding of the structure–performance relationship. For comparison, a sample denoted as FePO$_4$-MWCNTs was prepared by simply mixing the solid nanoparticles of FePO$_4$ and MWCNTs. Supplementary Figure S12 shows a TEM image of such a mixture in which the MWCNTs accounted for 24% in weight percentage, which was same as that of the MWCNTs@ 4-nm FePO$_4$ sample. The charge/discharge curves of all these four samples are shown in Figure 4a, and they show smooth slopes with no plateaus in the voltage range between 1.5 and 4.2 V, indicating a single-phase reaction route during the sodium ion insertion/extraction in the amorphous structure of FePO$_4$.[10] Interestingly, the core-shell structured samples were able to deliver a much higher discharge capacity compared with the one in form of the FePO$_4$-MWCNT mixture. Notably, the MWCNTs@ 4-nm FePO$_4$ sample showed the highest capacity of 120 mAh g^{-1}, whereas the FePO$_4$-MWCNTs sample could only produce a capacity of 55 mAh g^{-1}. Furthermore, we also observed a direct relationship between the shell structure and its battery performance. An increase in the shell thickness proved to be detrimental to the full realization of the discharge capability of FePO$_4$. Typically, the sample with the 12-nm FePO$_4$ coating layer showed a performance similar to the FePO$_4$-MWCNT mixture, which was much less than the samples with thinner coatings. Generally, to achieve a higher capacity for the active FePO$_4$ value, a much thinner coating is necessary. We attempted to synthesize a 2-nm FePO$_4$ shell by reducing the amount of Fe^{3+} and HPO_4^{2-} for the surface coating (Supplementary Figure S13). The sample did show an improved capacity of approximately 160 mAh g^{-1} if the mass of FePO$_4$ alone was considered. However, due to the complex nature of the CNT surface (including the curved structure and the uncontrolled surface properties from the acid treatment step), achieving a uniform coating
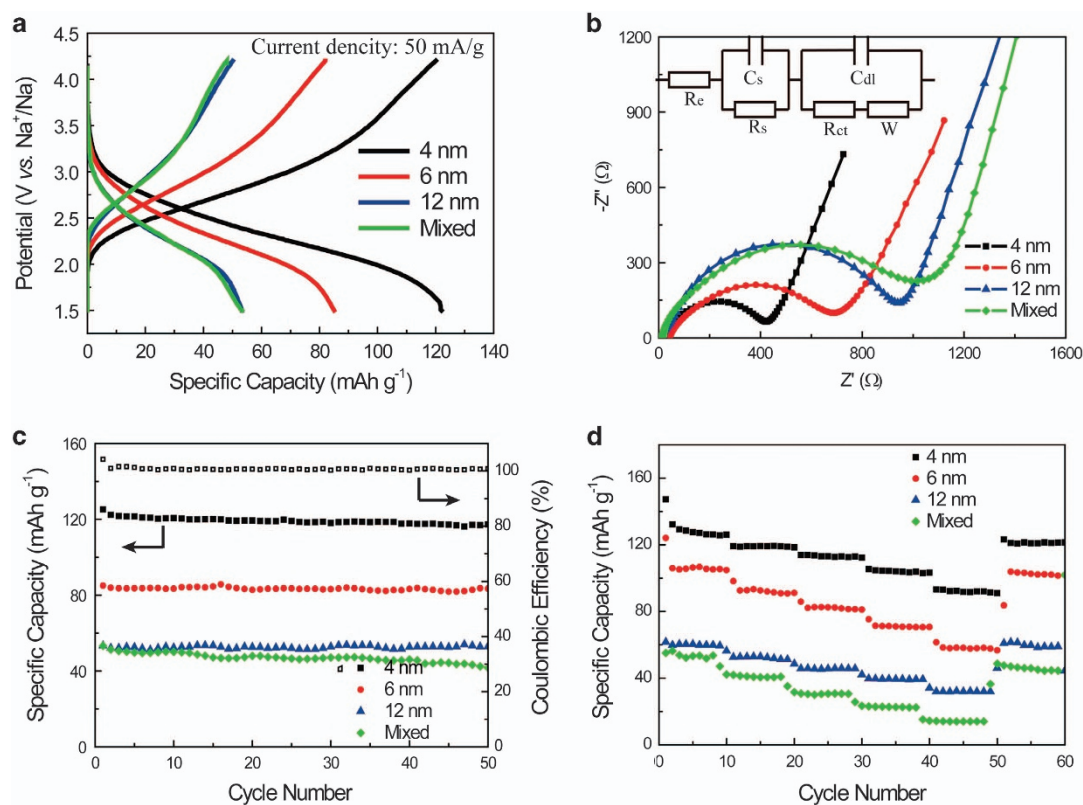
Figure 4 Electrochemical characterization of the MWCNTs@FePO$_4$ cathode material: galvanostatic charging/discharging profiles operated at 1.5–4.2 V with a current density of 50 mA g^{-1} (**a**); electrochemical impedance spectrum (EIS) and its equivalent electric circuit (**b**); cycling performance performed at a current density of 50 mA g^{-1}, dots represent the discharge capacity and squares represent the columbic efficiency (**c**); and rate capability at current densities of 20, 50, 100, 200 and 500 mAh g^{-1} (**d**).

of FePO$_4$ when its surface layer was as low as 2 nm was hardly achieved (Supplementary Figure S13a). Therefore, in Figure 4, we only present the data from samples with uniform coatings for a clear comparison.

Electrochemical impedance spectroscopy was used to obtain a better understanding of the structure-related performance. We recorded the electrochemical impedance spectra for all four samples mentioned above (Figure 4b), and their Nyquist plots were different from each other, especially regarding the radius of the semicircle in the high-to-medium frequency range, which was related to the charge transfer and surface film resistance (R_{ct}) during the cation interfacial transfer between the electrode material and the electrolyte.[14] The fitting result of the electrochemical impedance spectroscopy test showed that R_{ct} decreased as the FePO$_4$ thickness decreased (Supplementary Table S2). Not surprisingly, an increase in the thickness of the surface coating layer made the charge transfer on the interface harder due to the poor electronic conductivity of the amorphous FePO$_4$ shell, which was expected to induce a higher polarization for thicker layers and produced inferior electrochemical performance compared with the thinner layers. To further investigate the kinetics of the Na$^+$ transport, the chemical diffusion coefficient of Na$^+$ (D_{Na}) was calculated from the cyclic voltammetry tests. As shown in Supplementary Table S3, the thicker FePO$_4$ coating hampered the transport of Na$^+$, and it was critical to maintain the surface shell at a thin state to facilitate satisfactory mobility for Na$^+$.

The cyclability of the FePO$_4$-based cathodes was tested, and the results are shown in Figure 4c. The MWCNTs@FePO$_4$ samples showed a very stable performance regarding the discharge capability.

For the 4-nm FePO$_4$-coated sample, it retained a discharge capacity of 115 mAh g^{-1} after 50 cycles at a current of 50 mA g^{-1}, which was approximately 96% of its initial capacity, and it showed good capability for a stable output. Meanwhile, its columbic efficiency was constant at approximately 100% after the initial stage of electrode activation during the first cycle. Figure 4d shows the battery performance of the different samples at different c-rates. Obviously, the FePO$_4$ in the form of a nanoshell on the MWCNTs exhibited a much improved rate capability compared with the simple mixture of these two components. Additionally, the MWCNTs@ 4-nm FePO$_4$ was identified as the best sample, with specific capacities of 125 mAh g^{-1} at 20 mA g^{-1}, 120 mAh g^{-1} at 50 mA g^{-1}, 110 mAh g^{-1} at 100 mA g^{-1}, 100 mAh g^{-1} at 200 mA g^{-1} and 90 mAh g^{-1} at 500 mA g^{-1}, indicating promising high-rate performance. Meanwhile, the control sample only delivered a discharge capability of 55 mAh g^{-1} at 20 mA g^{-1}, 40 mAh g^{-1} at 50 mA g^{-1}, 30 mAh g^{-1} at 100 mA g^{-1}, 25 mAh g^{-1} at 200 mA g^{-1}, and 15 mAh g^{-1} at 500 mA g^{-1}. The contrast between these two types of samples clearly highlighted the advantage of the core-shell configuration. As expected, such a cable-like structure was able to guarantee an intimate contact between the FePO$_4$ and MWCNTs, which allowed the fast transport of electrons possible to achieve a favorable battery performance compared with the FePO$_4$-MWCNT mixture.

CONCLUSION

We reported a simple and easy synthetic protocol for the construction of FePO$_4$-based core-shell structures. By tuning the growth kinetics of FePO$_4$ in an aqueous solution, we were able to coordinate its

precipitation into a heterogeneous growth mode, forming uniform nanoshells onto a large variety of substrates. We also demonstrated the possibility of precisely regulating the shell thickness through an orchestrated effort in reaction control. We applied this synthetic strategy for the construction of an electrode material using MWCNTs as a unique conductive core. We demonstrated that a nanocomposite of MWCNTs@FePO$_4$ was promising for its application as a cathode material in SIBs due to both the highly conductive core and the electrochemically active shell, which exhibited a high discharge capacity and a much improved rate capability. We anticipate that our progress in FePO$_4$ control will offer new potential in different research fields, such as materials chemistry, catalysis and energy storage devices.

CONFLICT OF INTEREST

The authors declare no conflict of interest.

ACKNOWLEDGEMENTS

1 Palomares, V., Serras, P., Villaluenga, I., Hueso, K. B., Carretero-Gonzalez, J. & Rojo, T. Na-ion batteries, recent advances and present challenges to become low cost energy storage systems. *Energy Environ. Sci.* **5**, 5884–5901 (2012).

2 Han, M.-H., Gonzalo, E., Singh, G. & Rojo, T. A comprehensive review of sodium layered oxides: powerful cathodes for Na-ion batteries. *Energy Environ. Sci.* **8**, 81–102 (2015).

3 Kundu, D., Talaie, E., Duffort, V. & Nazar, L. F. The emerging chemistry of sodium ion batteries for electrochemical energy storage. *Angew. Chem. Int. Ed.* **54**, 3431–3448 (2015).

4 Slater, M.-D., Kim, D., Lee, E. & Johnson, C.-S. Sodium-ion batteries. *Adv. Funct. Mater.* **23**, 947–958 (2013).

5 Yuan, S., Liu, Y.-B., Xu, D., Ma, D.-L., Wang, S., Yang, X.-H., Cao, Z.-Y. & Zhang, X.-B. Pure single-crystalline Na$_{1.1}$V$_3$O$_{7.9}$ nanobelts as superior cathode materials for rechargeable sodium-ion batteries. *Adv. Sci.* **2**, 1400018 (2015).

6 Zhu, H., Jia, Z., Chen, Y., Weadock, N., Wan, J., Vaaland, O., Han, X., Li, T. & Hu, L. Tin anode for sodium-ion batteries using natural wood fiber as a mechanical buffer and electrolyte reservoir. *Nano Lett.* **13**, 3093–3100 (2013).

7 Chao, D., Zhu, C., Xia, X., Liu, J., Zhang, X., Wang, J., Liang, P., Lin, J., Zhang, H., Shen, Z.-X. & Fan, H.-J. Graphene quantum dots coated VO$_2$ arrays for highly durable electrodes for Li and Na ion batteries. *Nano Lett.* **15**, 565–573 (2015).

8 Ponrouch, A. & Palacin, M.-R. On the high and low temperature performances of Na-ion battery materials: hard carbon as a case study. *Electrochem. Commun.* **54**, 51–54 (2015).

9 Fang, Y., Xiao, L., Qian, J., Ai, X., Yang, H. & Cao, Y. Mesoporous amorphous FePO$_4$ nanospheres as high-performance cathode material for sodium-ion batteries. *Nano Lett.* **14**, 3539–3543 (2014).

10 Liu, Y., Xu, Y., Han, X., Pellegrinelli, C., Zhu, Y., Zhu, H., Wan, J., Chung, A.-C., Vaaland, O., Wang, C. & Hu, L. Porous amorphous FePO$_4$ nanoparticles connected by single-wall carbon nanotubes for sodium ion battery cathodes. *Nano Lett.* **12**, 5664–5668 (2012).

11 Mathew, V., Kim, S., Kang, J., Gim, J., Song, J., Baboo, J.-P., Park, W., Ahn, D., Han, J., Gu, L., Wang, Y., Hu, Y.-S., Sun, Y.-K. & Kim, J. Amorphous iron phosphate: potential host for various charge carrier ions. *NPG Asia Mater.* **6**, e138 (2014).

12 Prosini, P.-P., Lisi, M., Scaccia, S., Carewska, M., Cardellini, F. & Pasquali, M. Synthesis and characterization of amorphous hydrated FePO$_4$ and its electrode performance in lithium batteries. *J. Electrochem. Soc.* **1**, A297 (2002).

13 Santic, B., Mogus-Milankovic, A. & Day, D.-E. The dc electrical conductivity of iron phosphate glasses. *J. Non-Cryst. Solids* **296**, 65–73 (2001).

14 Liu, Y., Xu, S., Zhang, S., Zhang, J., Fan, J. & Zhou, Y. Direct growth of FePO$_4$/reduced graphene oxide nanosheet composites for the sodium-ion battery. *J. Mater. Chem. A* **3**, 5501–5508 (2015).

15 Xu, S., Zhang, S., Zhang, J., Tan, T. & Liu, Y. A maize-like FePO$_4$@MCNT nanowire composite for sodium-ion batteries *via* a microemulsion technique. *J. Mater. Chem. A* **2**, 7221–7228 (2014).

16 Fu, Y., Su, Y.-S. & Manthiram, A. Li$_2$S-carbon sandwiched electrodes with superior performance for lithium-sulfur batteries. *Adv. Energy Mater.* **4**, 1300655–130659 (2014).

17 Cheng, J.-P., Yu, J., Shi, D., Wang, D.-S., Liu, Y.-F., Liu, F., Zhang, X.-B. & Li, J.-G. Controllable one-step synthesis of magnetite/carbon nanotubes composite and its electrochemical properties. *Appl. Phys. A-Mater* **106**, 837–842 (2012).

18 Kim, S. W., Ryu, J., Park, C. B. & Kang, K. Carbon nanotube-amorphous FePO$_4$ core–shell nanowires as cathode material for Li ion batteries. *Chem. Commun.* **46**, 7409–7411 (2010).

19 Cai, R., Liu, H., Zhang, W., Tan, H., Yang, D., Huang, Y., Hng, H.-H., Lim, T.-M. & Yan, Q. Controlled synthesis of double-walla-FePO$_4$ nanotubes and their LIB cathode properties. *Small* **9**, 1036–1041 (2013).

20 Yin, Y., Wu, P., Zhang, H. & Cai, C. Enhanced cathode performances of amorphous FePO$_4$ hollow nanospheres with tunable shell thickness in lithium ion batteries. *Electrochem. Commun.* **18**, 1–3 (2012).

21 Chaudhuri, R.-G. & Paria, S. Core/shell nanoparticles: classes, properties, synthesis mechanisms, characterization, and applications. *Chem. Rev.* **112**, 2373–2433 (2012).

22 Liu, R., Mi, S., Li, Y., Chen, C., Xie, Y., Chen, Q. & Chen, Z. Synthesis of monodispersed Fe$_3$O$_4$@C core/shell nanoparticles. *Sci. China-Chem.* **59**, 394–397 (2016).

23 Lu, P., Li, J., Wang, D. & Wan, L.-J. Si@Cu@Au AFM tips for tip-enhanced raman spectrum. *Sci. China-Chem.* **58**, 1494–1500 (2015).

24 Li, G. & Tang, Z. Noble metal nanoparticle@metal oxide core/yolk–shell nanostructures as catalysts: recent progress and perspective. *Nanoscale* **6**, 3995–4011 (2014).

25 McCann, J.-T., Li, D. & Xia, Y.-N. Electrospinning of nanofibers with core-sheath, hollow, or porous structures. *J. Mater. Chem.* **15**, 735–738 (2005).

26 Meng, Y., Zhao, Y., Hu, C., Cheng, H., Hu, Y., Zhang, Z., Shi, G. & Qu, L. All-graphene core-sheath microfibers for all-solid-state, stretchable fibriform supercapacitors and wearable electronic textiles. *Adv. Mater.* **25**, 2326–2331 (2013).

27 Li, G., Yang, Z. & Yang, W. Effect of FePO$_4$ coating on electrochemical and safety performance of LiCoO$_2$ as cathode material for Li-ion batteries. *J. Power Sources* **183**, 741–748 (2008).

28 Liu, J., Xiao, B., Banis, M.-N., Li, R., Sham, T.-K. & Sun, X. Atomic layer deposition of amorphous iron phosphates on carbon nanotubes as cathode materials for lithium-ion batteries. *Electrochim. Acta* **162**, 275–281 (2015).

29 Richardson, J. J., Björnmalm, M. & Caruso, F. Technology-driven layer-by-layer assembly of nanofilms. *Science* **348**, aaa2491-1–aaa249-11 (2015).

30 Li, M., Sun, L., Sun, K., Wang, R. & Xie, H. An optimum route to prepare FePO$_4$ center dot 2H$_2$O and its use as an iron source to synthesize LiFePO$_4$. *Sci. China-Chem.* **56**, 576–582 (2013).

31 Ferrari, A.-C. Raman spectroscopy of graphene and graphite: disorder, electron-phonon coupling, doping and nonadiabatic effects. *Solid State Comm.* **143**, 47–57 (2007).

32 Dresselhaus, M.-S., Dresselhaus, G., Saito, R. & Jorio, A. Raman spectroscopy of carbon nanotubes. *Phys. Rep.* **409**, 47–99 (2005).

33 Hong, Y. S., Ryu, K. S., Park, Y. J., Kim, M. G., Lee, J. M. & Chang, S. H. Amorphous FePO$_4$ as 3V cathode material for lithium secondary batteries. *J. Mater. Chem.* **12**, 1870–1874 (2002).

Supplementary Information accompanies the paper on the NPG Asia Materials website (http://www.nature.com/am)